

# Hybrid guiding: A multi-resolution refinement approach for semantic segmentation of gigapixel histopathological images

André Pedersen<sup>a,b,\*</sup>, Erik Smistad<sup>c,d</sup>, Tor V. Rise<sup>a,e</sup>, Vibeke G. Dale<sup>a,e</sup>, Henrik S. Pettersen<sup>a,e</sup>, Tor-Arne S. Nordmo<sup>f</sup>, David Bouget<sup>d</sup>, Ingerid Reinertsen<sup>c,d</sup>, Marit Valla<sup>a,b,e,g</sup>

<sup>a</sup>Department of Clinical and Molecular Medicine, Norwegian University of Science and Technology, NO-7491 Trondheim, Norway

<sup>b</sup>Clinic of Surgery, St. Olavs Hospital, Trondheim University Hospital, NO-7030 Trondheim, Norway

<sup>c</sup>Department of Circulation and Medical Imaging, Norwegian University of Science and Technology, NO-7491 Trondheim, Norway

<sup>d</sup>Department of Health Research, SINTEF Digital, NO-7465 Trondheim, Norway

<sup>e</sup>Department of Pathology, St. Olavs Hospital, Trondheim University Hospital, NO-7030 Trondheim, Norway

<sup>f</sup>Department of Computer Science, UiT The Arctic University of Norway, NO-9019 Tromsø, Norway

<sup>g</sup>Clinic of Laboratory Medicine, St. Olavs hospital, Trondheim University Hospital, NO-7030 Trondheim, Norway

---

## Abstract

Over the past decades, histopathological cancer diagnostics has become more complex, and the increasing number of biopsies is a challenge for most pathology laboratories. Thus, development of automatic methods for evaluation of histopathological cancer sections would be of value.

In this study, we used 624 whole slide images (WSIs) of breast cancer from a Norwegian cohort. We propose a cascaded convolutional neural network design, called H2G-Net, for semantic segmentation of gigapixel histopathological images. The design involves a detection stage using a patch-wise method, and a refinement stage using a convolutional autoencoder. To validate the design, we conducted an ablation study to assess the impact of selected components in the pipeline on tumour segmentation.

Guiding segmentation, using hierarchical sampling and deep heatmap refinement, proved to be beneficial when segmenting the histopathological images. We found a significant improvement when using a refinement network for post-processing the generated tumour segmentation heatmaps. The overall best design achieved a Dice score of  $0.933 \pm 0.069$  on an independent test set of 90 WSIs. The design outperformed single-resolution approaches, such as cluster-guided, patch-wise high-resolution classification using MobileNetV2 ( $0.872 \pm 0.092$ ) and a low-resolution U-Net ( $0.874 \pm 0.128$ ). In addition, the design performed consistently on WSIs across all histological grades and segmentation on a representative  $\times 400$  WSI took  $\sim 58$  seconds, using only the central processing unit.

The findings demonstrate the potential of utilizing a refinement network to improve patch-wise predictions. The solution is efficient and does not require overlapping patch inference or ensembling. Furthermore, we showed that deep neural networks can be trained using a random sampling scheme that balances on multiple different labels simultaneously, without the need of storing patches on disk. Future work should involve more efficient patch generation and sampling, as well as improved clustering.

**Keywords:** Hybrid guiding, Refinement network, Deep learning, Digital pathology, Hierarchical sampling, Clustering

---

## 1. Introduction

Cancer is an important cause of death, and of all cancers, breast cancer has the highest incidence worldwide (Ferlay *et al.*, 2020). Cancer diagnostics is based on clinical examination, medical imaging and histopathological assessment of the tumour. The latter includes analysis

of specific biomarkers that often guides treatment of the patients. Most pathology laboratories are burdened by an increasing number of biopsies and more complex diagnostics (The Royal College of Pathologists, 2018). To reduce workload for pathologists, automatic assessment of tumours and biomarkers would be of value.

A natural first step in automatic tumour and biomarker analysis would be to correctly identify the lesion, thus separating the tumour from surrounding tissue. For automatic biomarker assessment, it is important to ensure that biomarker status is obtained exclusively in the invasive epithelial cancer cells.

With the promise of deep learning-based methods in computational pathology (Srinidhi *et al.*, 2021), accurate segmentation of the cancer region would be beneficial for

---

**Abbreviations:** WSI - whole slide image, CNN - convolutional neural network, PCA - principal component analysis, CAE - convolutional autoencoder, GUI - graphical user interface, GPU - graphics processing unit, CPU - central processing unit, Mob - MobileNetV2, Inc - InceptionV3, AN - annotation, BCS - Breast Cancer Subtypes, H&E - hematoxylin-eosin, PW - patch-wise, LR - low-resolution, DSC - dice similarity coefficient, MIL - multiple instance learning.

\*Corresponding author

E-mail address: andre.pedersen@ntnu.no (André Pedersen)

building new classifiers and facilitate other cancer analysis methods.

In this study, we aim to develop and validate an efficient and accurate method for automatic segmentation of invasive breast cancer tumours in histopathological whole slide images (WSIs).

### 1.1. Related work

Processing histopathological WSIs is challenging due to their large size. WSIs captured at  $\times 400$  magnification may be as large as  $200k \times 100k$  pixels, and as such, cannot be used directly as input to convolutional neural networks (CNNs). A solution is to downsample the image to a size that is manageable for the CNN. However, this results in loss of information and is therefore often not useful for tumour segmentation. Another widely used approach is to divide the image into smaller patches (Aresta *et al.*, 2019), before each patch is sent to an algorithm to produce an output. The results are then stitched to form a complete segmentation or heatmap of the entire WSI. However, the use of such a patch-wise design based on high-resolution information only, often results in edge artifacts and poor global segmentation of larger structures (Priego Torres *et al.*, 2020).

Schmitz *et al.* (2021) compared multi-scale convolutional autoencoder (CAE) designs, applied in a patch-wise fashion across liver tumours in WSIs. They found that the network benefited significantly from the added multi-scale information, compared to the baseline U-Net (Ronneberger *et al.*, 2015). They also proposed non-overlapping inference to reduce runtime at the cost of reduced accuracy along patch edges. For handling these edge artifacts, Priego Torres *et al.* (2020) proposed a conditional random field-based, patch-wise, merging scheme.

To improve the patch-wise design, Guo *et al.* (2019) developed a multi-task network for classification and semantic segmentation of breast cancer. They used a pretrained InceptionV3 (Szegedy *et al.*, 2016) architecture and finetuned it on the Camelyon16 data set (Ehteshami Bejnordi *et al.*, 2017). Such transfer learning has the benefit of making training more efficient, as the network is not trained from scratch. Using a more complex backbone, such as InceptionV3, has the potential benefit of improved performance. However, the architecture is computationally expensive, and might therefore not be suitable for real-time applications, such as histopathological diagnostics.

Breast cancers are known for their intra- and intertumour heterogeneity, and thus their morphological appearance varies both within and between tumours. Due to intratumour heterogeneity, the patches generated from a single WSI often contain different tissue types and a varying morphological appearance. Qaiser *et al.* (2019) studied the effect of smart patch selection and balancing in preprocessing, to produce models that performed well on varying types of tissue. They demonstrated that a deep clustering approach of patches outperformed the conventional  $k$ -means (Steinhaus, 1956) clustering method.

A similar cluster-guiding strategy was performed by Yao, Zhu, and Huang (2019) using multiple instance learning. They used a pretrained VGG19-encoder (Simonyan and Zisserman, 2015) for feature extraction. The dimensionality of the features was reduced using principal component analysis (PCA) (Karl Pearson, 1901), before performing  $k$ -means clustering. Samples were drawn from these clusters and balanced during training. The number of clusters was set to four, as they assumed that there were four main natural tissue types in the data.

### 1.2. Architecture design

For image classification, MobileNetV2 (Sandler *et al.*, 2018) and InceptionV3 (Szegedy *et al.*, 2016) are popular baseline architectures, benchmarked on the ImageNet Large Scale Visual Recognition Challenge (ILSVRC) data set (Russakovsky *et al.*, 2015). Both architectures are commonly used in digital pathology (Aresta *et al.*, 2019; Kasani *et al.*, 2019; Skrede *et al.*, 2020).

For image segmentation, various CAE architectures have been proposed. The most commonly used CAE is *U-Net* (Ronneberger *et al.*, 2015), which is a fully-convolutional, symmetric, encoder-decoder network, including skip connections at each pooling level to efficiently produce refined segmentations. Recently, multi-scale architectures have been proposed as they can potentially extract information at different magnification levels in a more efficient and controlled manner compared to traditional CAEs (Kamnitsas *et al.*, 2017).

To further improve the multi-scale design, deep supervision has been proposed (Nie *et al.*, 2017). By combining multi-scale input with deep supervision, the segmentation task is guided by introducing a loss at each decoder level. By forcing the network to learn representative features at all resolution levels, one aims to produce a network that better develops an understanding of the object of interest.

In addition to multi-scale designs, attention-based CAEs have become popular (Minaee *et al.*, 2021). Using attention, the network learns to filter irrelevant image features or regions, thus making it more focused on the task at hand. Two commonly used attention designs are channel-wise and position attention. Two modern multi-scale, attention-based CAEs are *AGU-Net* and *DAGU-Net* (Bouget *et al.*, 2021), which use single and dual attention, respectively. Both architectures also use deep supervision.

Performing both detection and semantic segmentation in a single step is challenging. Often, the segmentation result is suboptimal and a post-processing method is required. Refinement networks for the CAE itself have therefore been proposed, either end-to-end (Jha *et al.*, 2020) or in multiple steps (Painchaud *et al.*, 2019). The end-to-end architecture, *DoubleU-Net*, is a cascaded U-Net design, where the output from the first network is sent as input to the latter, concatenated with the original input. Skip connection is then performed across the two CAEs to

map learned encoder features from the initial network to the latter.

### 1.3. FastPathology

We have previously developed the open-source platform FastPathology (Pedersen *et al.*, 2021), for deep learning-based digital pathology. It enables deployment of deep learning solutions on WSIs through a graphical user interface (GUI). Integration of new models and pipelines does not require coding and programming skills. The software supports a wide range of multi-input/output CNN architectures, such as MobileNetV2, U-Net and YOLOv3 (Redmon and Farhadi, 2018). Several inference engines are also supported, such as TensorRT (NVIDIA, 2019), OpenVINO (Intel, 2019) and TensorFlow (Abadi *et al.*, 2016). Through the ONNX (Bai *et al.*, 2019) format, models can be executed using TensorRT or OpenVINO, both of which are among the fastest for graphics processing unit (GPU) (NVIDIA) and central processing unit (CPU) (Intel) inference.

### 1.4. Contributions

In this paper, we present the following contributions:

- (1) A novel hierarchically-balanced, random sampling scheme that extracts patches directly from the WSI.
- (2) A concurrent clustering method performed during training, without the need to store temporary results, using a novel cluster-guided loss function.
- (3) A refinement network which combines high-resolution information and global information, producing superior performance over single resolution approaches.
- (4) The proposed pipeline and trained models are made openly available for use in *FastPathology* (Pedersen *et al.*, 2021).
- (5) The code to reproduce the experiments is made openly available on GitHub: <https://github.com/andrepd/H2G-Net>.

## 2. Materials and methods

### 2.1. Data set and annotation design

In this study, we used 4  $\mu\text{m}$  thick whole sections ( $n=624$ ) from a cohort of Norwegian breast cancer patients (Engström *et al.*, 2013), Breast Cancer Subtypes 1 (BCS-1). All tumours were previously classified into histological grade, according to the Nottingham grading system (Elston and Ellis, 1991). The sections were stained with hematoxylin-eosin (H&E), scanned at  $\times 400$  magnification using an Olympus scanner BX61VS with VSI120-S5, and stored in the cellSens VSI format using JPEG2000 compression.

For each WSI, the tumour area was delineated by pathologists using QuPath (Bankhead *et al.*, 2017). To speed up and assist with the annotation work, automatic

and semi-automatic approaches were tested, similarly to the approach used by Carse and McKenna (2019). We used two different approaches for annotation (AN1 and AN2). For both annotation designs, predicted annotations were manually adjusted by the pathologists using the brush tool in QuPath.

The first 150 WSIs were annotated using the AN1 method, which involved using the semi-automatic tissue detection function in QuPath. The following parameters were used for performing segmentation: simple tissue detection threshold 200, requested pixel size 20, and minimum area 100,000. In cases where the algorithm failed, the parameters were adjusted or the tumour was manually annotated from scratch.

The remaining WSIs ( $n=474$ ) were annotated using the AN2 method (see Figure 1). A patch-wise CNN, similar to the Inc-PW method described in Section 3.2, was trained from a subset of the first 150 annotated WSIs. The model was trained in Python, and the produced model was then applied to the remaining WSIs. The resulting heatmaps were imported in QuPath and converted to annotations. Simple morphological post-processing was then performed before the segmentations were adjusted by the pathologists.

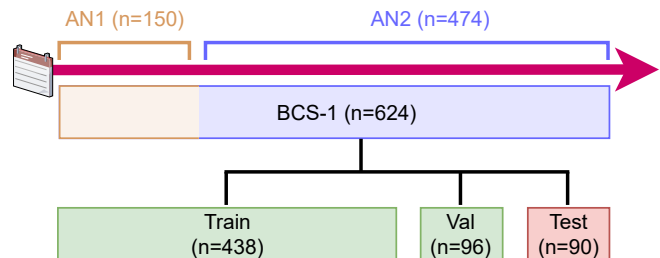


Figure 1: Description of the data generation timeline and process. The 624 WSIs were annotated with two different annotation methods (AN1 and AN2). The data set was then randomly split into train, validation, and test sets. AN: Annotation, BCS: Breast Cancer Subtypes. Val: Validation.

Finally, to ensure consistency, all annotations were reviewed by a single pathologist experienced in breast cancer pathology and minor adjustments were made.

The pathologists' annotations were exported from QuPath as individual PNGs, one for each WSI, with a down-sampling factor of four. The PNGs were then converted to tiled, pyramidal TIFFs, using the command line tool `vips`<sup>1</sup>, with tiles sized  $1024 \times 1024$  and a LZW lossless compression. All WSIs were converted to the single-file, pyramidal tiled, generic TIFF format using the command line tool `vsi2tif`<sup>2</sup>.

Lastly, the annotated WSIs were randomly distributed into the three sets: training ( $\sim 70\%$ ;  $n=438$ ), validation ( $\sim 15\%$ ;  $n=96$ ), and test ( $\sim 15\%$ ;  $n=90$ ) set.

<sup>1</sup><https://github.com/libvips/libvips>

<sup>2</sup><https://github.com/andrepd/vsi2tif>

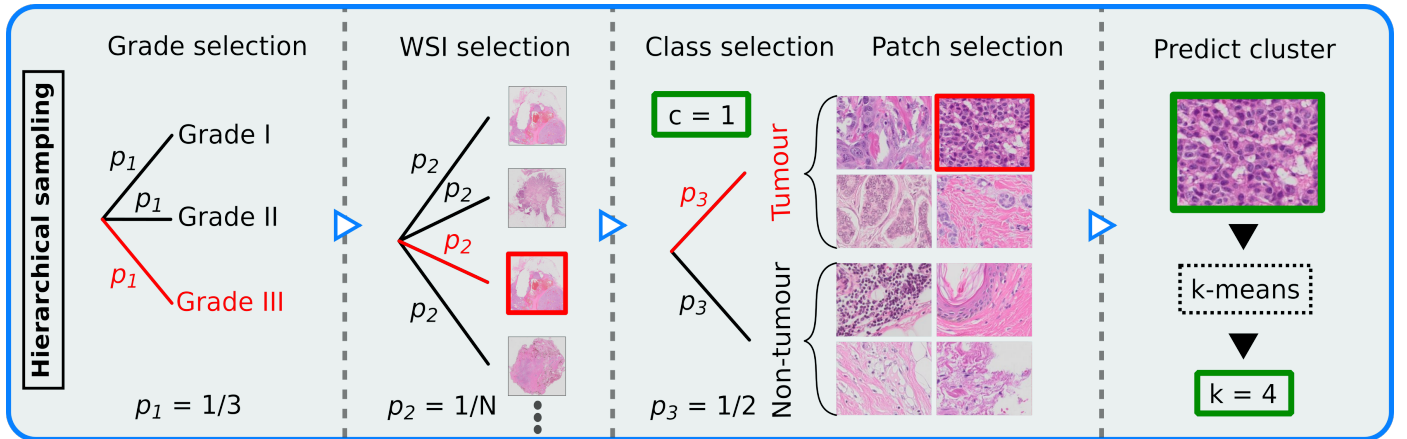


Figure 2: Illustration of the hierarchical sampling scheme, demonstrating how patches were sampled from the  $N$  whole slide images (WSIs) for training the patch-wise model. Sampling was conducted as a uniform tree diagram. Thus,  $p_i$  represents probability at step  $i \in \{1, 2, 3\}$ . A potential path for patch selection is marked red. Each patch was assigned a class label  $c$  (tumour or non-tumour) and a cluster  $k$  (ten different clusters). Each output is marked in green.

## 2.2. Preprocessing

Following annotation, we extracted patches sized  $256 \times 256$  at  $\times 100$  magnification level from the WSIs. Only patches containing more than 25% tissue were included. Patches with more than 25% tumour were considered tumour patches, and only patches with no tumour were considered non-tumour. The remaining patches in the range (0, 25%] tumour tissue were discarded. For each WSI, the coordinates of accepted patches were stored along with the assigned label i.e. non-tumour/tumour.

## 2.3. Hierarchical sampling scheme

A batch generator was created to sample patches directly from the raw WSI format. Patches were read using OpenSlide (Satyanarayanan *et al.*, 2013), which enabled multi-threading processing. The generator was based on the condition that it is important to balance patches according to the following features: class label, tissue type, tissue and tumour area, and histological grade.

Patches were sampled in a hierarchical sampling scheme (see Figure 2), conducted as a tree structure uniformly distributed at each respective stage. The goal was to make all relevant outcomes equally probable. The sampling scheme was defined in the ordered stages: 1) Randomly select a histological grade, 2) from the grade select a WSI, 3) from the WSI select a class label, 4) from the class label select a patch.

To include patch-level tissue type label in the balancing scheme, we used our sampling generator to train a  $k$ -means clustering model, similar to Yao, Zhu, and Huang (2019). From a set of 100 batches of size 32, features were extracted using a VGG-16 (Simonyan and Zisserman, 2015) backbone pretrained on the ImageNet data set (Deng *et al.*, 2009). The extracted features were then standardized using Z-score normalization, before PCA was performed. The number of principal components was chosen such that

95% of the variance of the data was explained. The  $k$ -means model was then trained using  $k = 10$  number of clusters, as recommended in a related study (Yao, Zhu, Jonnagaddala, *et al.*, 2020). The clustering model was implemented using the Python library `scikit-learn` (Pedregosa *et al.*, 2011).

To utilize the trained clustering model in the patch-wise CNN, TensorFlow equivalents of the standardization, PCA and  $k$ -means transform methods were implemented, which was defined as a TensorFlow graph. The scikit-learn trained weights were then loaded for each corresponding component.

Finally, for training the CNN classifier, each patch was passed through two different graphs; I) a frozen pipeline that performed clustering and II) a learnable deep neural network that performed classification. The outputs from both models were then passed to the loss function.

The MobileNetV2 architecture was used for the patch-wise CNN classification of breast cancer tumour tissue, as it is lightweight, efficient, and optimized for low-end processors and thus suitable for real-time deployment. To further reduce the number of parameters, we simplified the classifier head. The updated classifier contained a global average pooling layer, followed by a dense layer of 100 hidden neurons, dropout (Srivastava *et al.*, 2014) with a 50% drop rate, ReLU activation, batch normalization (Ioffe and Szegedy, 2015), and finally a dense layer with softmax activation function.

## 2.4. Cluster-guided loss function

To balance on tissue type and thus ensure similar model performance on all predicted clusters, we included the cluster-information in the loss computation. For a given batch, we calculated the cross-entropy loss for each cluster independently, and then calculated the macro average across each cluster. We named this loss function cluster-weighted categorical cross-entropy (CWCE) loss. The loss



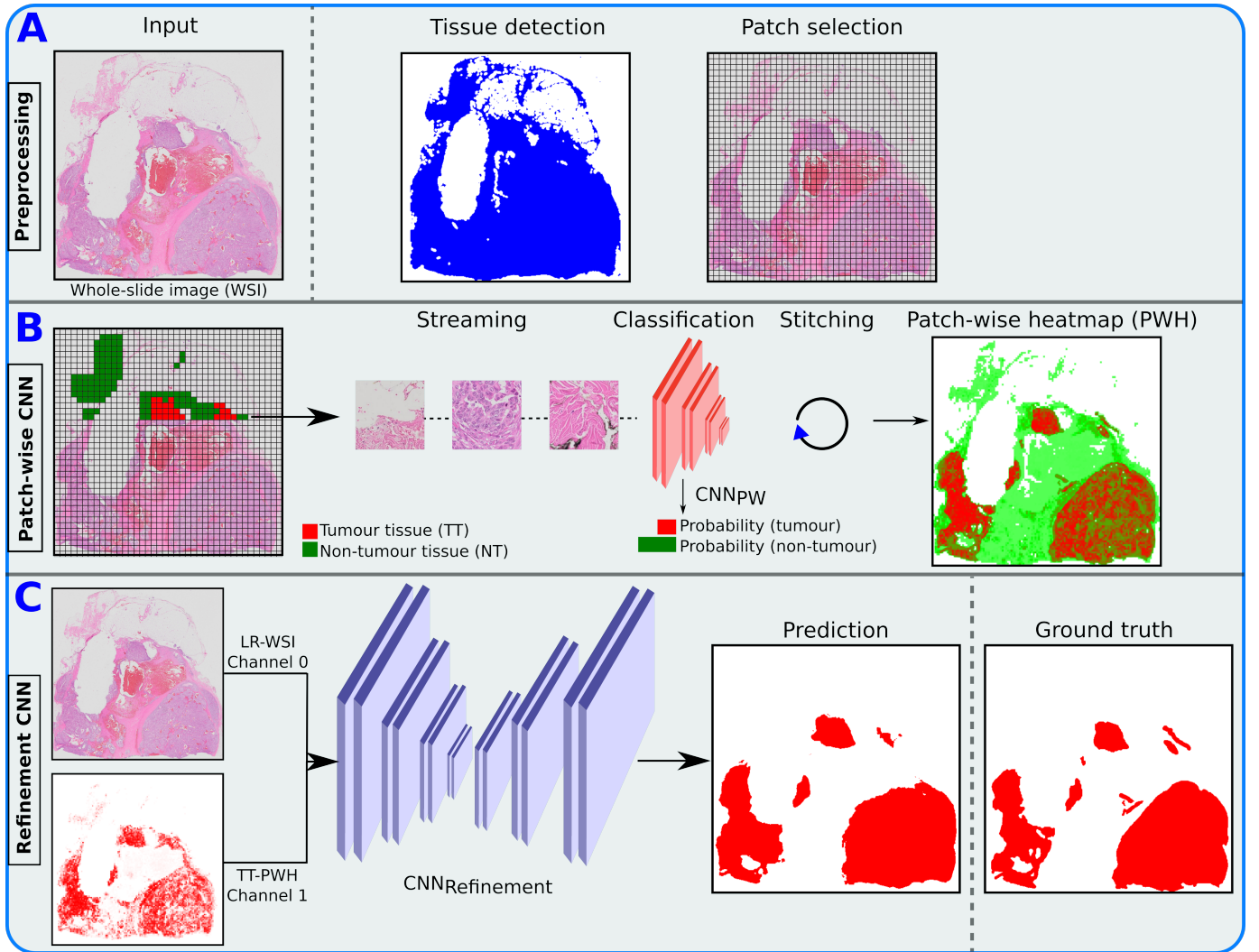


Figure 3: Illustration of the inference pipeline, from the whole slide image (WSI) to the final tumour segmentation (prediction). A) Apply tissue detection before patch selection. B) Stream accepted patches through a trained patch convolutional neural network (CNN) classifier and stitch the output to form a patch-wise heatmap (PWH). C) Merge the low-resolution (LR) WSI with the resulting tumour tissue (TT) PWH and send it through the trained refinement CNN, using a probability threshold of 0.5, to produce the final prediction.

can be mathematically described as:

$$\mathcal{L}_{\text{CWCE}} = -\frac{1}{K_b} \sum_{k=1}^{K_b} \sum_{c=1}^C \sum_{i=1}^B \mathbb{1}(q_{i,k} = k) y_{i,c} \log(p_{i,c}) \quad (1)$$

where  $i \in \{1, \dots, B\}$  represents sample  $i$  in a batch of size  $B$ ,  $k \in \{1, \dots, K_b\}$  cluster in a mini-batch  $b$  of size  $B$  of  $K_b$  represented clusters,  $c \in \{1, \dots, C\}$  class,  $p$  class prediction,  $q$  cluster prediction, and ground truth tumour class. Note that the number of clusters  $K_b$  may vary between mini-batches.

### 2.5. Heatmap generation

The trained patch-wise model was then applied across the training and validation sets. Only patches assigned the tissue label were used (see Figure 3A). For each WSI, the trained model was applied in a non-overlapping, sliding window fashion, storing the resulting stitched confidence heatmap of the tumour class (see Figure 3B).

### 2.6. Refinement stage

To improve the result from the patch-wise detection, we combined the heatmap with the low-resolution WSI (see Figure 3C). This was done in an additional stage using a Refinement CNN. A suitable magnification level was chosen ( $\geq 1024 \times 1024$  pixels), and a low-resolution version of the original WSI was extracted from the image pyramid. The image was then normalized to  $[0, 1]$ , before both the resulting image and the heatmap were resized to  $1024 \times 1024$  using bilinear interpolation. A separate fully-convolutional neural network was then used to refine the resulting heatmaps from the detection stage. We used the U-Net (Ronneberger *et al.*, 2015) architecture, which took the concatenated low-resolution three-channel WSI and predicted heatmap as input.

### 2.7. From development to deployment

After training the patch-wise and refinement models, the models are ready to be used for inference. The inference pipeline is illustrated in Figure 3. The trained TensorFlow models were converted to the ONNX standard format, to enable efficient inference on both GPU and CPU with different frameworks. The models were then integrated into the FastPathology (Pedersen *et al.*, 2021) platform by writing a FAST (Smistad *et al.*, 2019) text pipeline, containing information about the inference pipeline and how the models should be handled (e.g., input shape, node names, and inference type). Thus, the proposed pipeline can be used through a GUI without programming. Binary release of FastPathology, trained models, test data, and source code can be accessed on GitHub<sup>3</sup>.

## 3. Validation study

### 3.1. Experiments

We conducted an ablation study to evaluate our design. The experiments conducted were:

1. To assess the importance of architecture complexity in breast cancer tumour detection in WSIs, we compared CNN classifiers using the two backbone architectures InceptionV3 and MobileNetV2.
2. To evaluate the cluster-guiding approach, we conducted experiments with and without  $k$ -means using the MobileNetV2 backbone.
3. To assess the effect of post-processing on the predicted heatmap, we compared state-of-the-art CAEs against simple baseline methods.
4. To evaluate the importance of having a GPU for inference, runtime measurements of the best performing method were performed with and without using the GPU.

### 3.2. Baseline segmentation methods

Using our pipeline, any architecture or component can be removed, added, or substituted. It is therefore valuable to assess the importance of each component in the pipeline. To evaluate the pipeline, we used existing, well-documented, state-of-the-art architectures. For patch-wise classification we used the MobileNetV2 ( $\sim 2.39$ M params.) and InceptionV3 ( $\sim 22.00$ M params.) backbones pre-trained on the ImageNet data set, and used the same simplified classifier head for both architectures, as described in Section 1.2.

For image segmentation refinement, we compared the CAE architectures U-Net ( $\sim 11.58$ M params.), AGU-Net ( $\sim 7.68$ M params.), DAGU-Net ( $\sim 9.99$ M params.), and DoubleU-Net (16.04M params.). In addition, we

included a traditional, widely used tissue segmentation method (Bándi *et al.*, 2019), to serve as a minimal baseline measure. This method simply segments all tissue, and thus all tuned methods should outperform it. For this method, the image was resized to  $1024 \times 1024$ , before being converted to the HSV (Hue, Saturation, Value) colour domain. Then, the saturation image was thresholded using Otsu’s method (Otsu, 1979).

The autoencoders were slightly modified to work better for our use case and data set. In depth details about modifications, as well as implementations for all architectures used, can be found on our GitHub repository<sup>4</sup>.

In summary, the following segmentation designs were compared:

- (I) **Otsu**: Intensity-based thresholding for tissue segmentation.
- (II) **UNet-LR**: Segmentation of low-resolution WSI using a U-Net architecture.
- (III) **Inc-PW**: Patch-wise classification using an InceptionV3 architecture.
- (IV) **Mob-PW**: Patch-wise classification using a MobileNetV2 architecture.
- (V) **Mob-KM-PW**: Same as (IV), with  $k$ -means guiding.
- (VI) **Mob-PW-UNet**: Same as (IV), with a U-Net refinement network.
- (VII) **Mob-PW-AGUNet**: Same as (IV), with an AGU-Net refinement network.
- (VIII) **Mob-PW-DAGUNet**: Same as (IV), with a DAGU-Net refinement network.
- (IX) **Mob-PW-DoubleUNet**: Same as (IV), with a DoubleU-Net refinement network.

### 3.3. Statistical evaluation

All patch-wise and refinement models were trained using the same training set, and the best models were selected based on the performance on the validation set. The test set was used as a hold-out sample for an unbiased, final evaluation.

A threshold of 0.5 was used to distinguish between the tumour and non-tumour classes. Metrics were reported WSI-wise, and only on the test set. For each respective metric, macro average and standard deviation were reported. The specific metrics used to assess performance were pixel-wise recall, precision, and the dice similarity coefficient (DSC). To further assess the robustness of the design, we also reported DSC for each histological grade.

We performed multiple pairwise Tukey’s range tests, comparing the DSC measures for all deep learning-based designs. The p-values were estimated for the test set (see Supplementary, Table S1).

<sup>3</sup><https://github.com/AICAN-Research/FAST-Pathology>

<sup>4</sup><https://github.com/andrepd/H2G-Net>

### 3.4. Training parameters

For training the classification models, we fine-tuned the respective pretrained backbones using the Adam optimizer (Kingma and Ba, 2014) with an initial learning rate of  $1e-4$ . For batch generation, 500 and 200 batches of size 64 for training and validation, respectively, were sampled randomly for each epoch. The models were trained for 100 epochs. Batches were generated in parallel using eight workers with a maximum queue size of 20. Models were trained using the following online data augmentation scheme of which all had a 50% chance of being used: random horizontal/vertical flip,  $90^\circ$  lossless rotations, HSV colour augmentation with a random shift of range  $[-20, 20]$ , and multiplicative brightness augmentation of range  $[0.8, 1.2]$ .

All segmentation models were trained from scratch using the Adam optimizer with an initial learning rate of  $1e-3$ . Accumulated gradients using a batch size of four with six accumulation steps were performed. For online data augmentation, simple horizontal/vertical flip,  $90^\circ$  rotations, random zoom of range  $[0.8, 1.2]$ , and Macenko (Macenko *et al.*, 2009) stain augmentation<sup>5</sup> using  $\sigma_1 = \sigma_2 = 0.1$ , with a chance of 50% of being used, were conducted. The models were trained for 1000 epochs, or until the early stopping criterion with a patience of 100 epochs was achieved.

Implementation was done in Python 3.6, and CNN architectures were implemented in TensorFlow (v1.13.1). Experiments were performed using an Intel Xeon Silver 3110 CPU, with 32 cores and 2.10 GHz, and an NVIDIA Quadro P5000 dedicated GPU.

## 4. Results

For the test set, all deep learning-based methods outperformed the tissue segmentation method, Otsu, in terms of DSC (see Table 1). Comparing the patch-wise classifiers, Inc-PW and Mob-PW, no significant difference in DSC was found between the architectures ( $p \approx 0.9$ , see Supplementary, Table S1). Adding cluster-guiding to Mob-PW, Mob-PW-KM, slightly reduced performance, however, not significantly ( $p \approx 0.9$ ).

Table 1: Test set segmentation performance for the different designs. DSC: Dice Similarity Coefficient, Inc: InceptionV3, Mob: MobileNetV2, PW: Patch-wise, KM:  $k$ -means, LR: Low-resolution. Results are reported as mean  $\pm$  standard deviation.

Designs	Recall	Precision	DSC
(I) Otsu	$0.990 \pm 0.027$	$0.534 \pm 0.200$	$0.669 \pm 0.179$
(II) UNet-LR	$0.931 \pm 0.113$	$0.851 \pm 0.165$	$0.874 \pm 0.128$
(III) Inc-PW	$0.881 \pm 0.118$	$0.909 \pm 0.099$	$0.887 \pm 0.089$
(IV) Mob-PW	$0.879 \pm 0.123$	$0.907 \pm 0.100$	$0.885 \pm 0.094$
(V) Mob-KM-PW	$0.853 \pm 0.124$	$0.909 \pm 0.097$	$0.872 \pm 0.092$
(VI) Mob-PW-UNet	$0.944 \pm 0.074$	<b><math>0.929 \pm 0.088</math></b>	<b><math>0.933 \pm 0.069</math></b>
(VII) Mob-PW-AGUNet	<b><math>0.954 \pm 0.066</math></b>	$0.909 \pm 0.097$	$0.927 \pm 0.072$
(VIII) Mob-PW-DAGUNet	$0.942 \pm 0.075$	$0.922 \pm 0.091$	$0.928 \pm 0.072$
(IX) Mob-PW-DoubleUNet	$0.949 \pm 0.073$	$0.919 \pm 0.093$	$0.929 \pm 0.074$

Among the best single-resolution designs (i.e. UNet-LR, Inc-PW, and Mob-PW), the patch-wise approaches performed slightly better in terms of DSC, but not significantly ( $p \approx 0.9$ ). The low-resolution approach (UNet-LR) achieved better recall, but with the cost of poorer precision.

Introducing a U-Net-inspired refinement network (using both the low-resolution WSI and the resulting heatmap from Mob-PW) resulted in significant improvement compared to the best single resolution approach (Mob-PW-UNet vs Inc-PW,  $p \approx 0.012$ ). All methods using a refinement network significantly outperformed the single resolution approaches.

Table 2: Test set segmentation performance for the different designs in histological grades I-III. DSC: Dice Similarity Coefficient, Inc: InceptionV3, Mob: MobileNetV2, PW: Patch-wise, KM:  $k$ -means, LR: Low-resolution. Results are reported as mean  $\pm$  standard deviation.

Designs	DSC (n=90)		
	Grade I (11)	Grade II (48)	Grade III (31)
(I) Otsu	$0.732 \pm 0.151$	$0.659 \pm 0.186$	$0.664 \pm 0.174$
(II) UNet-LR	$0.880 \pm 0.127$	$0.862 \pm 0.142$	$0.890 \pm 0.099$
(III) Inc-PW	$0.901 \pm 0.072$	$0.882 \pm 0.088$	$0.890 \pm 0.095$
(IV) Mob-PW	$0.887 \pm 0.089$	$0.882 \pm 0.092$	$0.890 \pm 0.100$
(V) Mob-KM-PW	$0.851 \pm 0.111$	$0.872 \pm 0.089$	$0.880 \pm 0.088$
(VI) Mob-PW-UNet	$0.936 \pm 0.073$	<b><math>0.931 \pm 0.058</math></b>	<b><math>0.935 \pm 0.083</math></b>
(VII) Mob-PW-AGUNet	$0.933 \pm 0.082$	$0.926 \pm 0.060$	$0.927 \pm 0.083$
(VIII) Mob-PW-DAGUNet	$0.935 \pm 0.075$	$0.926 \pm 0.058$	$0.929 \pm 0.088$
(IX) Mob-PW-DoubleUNet	<b><math>0.942 \pm 0.070</math></b>	$0.924 \pm 0.066$	$0.934 \pm 0.085$

Comparing the refinement architectures, the best performance in terms of precision and DSC was found from the U-Net design, Mob-PW-UNet, but the difference was not statistically significant ( $p \approx 0.9$  for all comparisons). No benefit of using more advanced CAE architectures was found.

When each histological grade was analyzed separately, Mob-PW-DoubleUNet was the best performing method for grade I and Mob-PW-UNet performed best on grade II and III (see Table 2). All designs guided by the hierarchical sampling scheme (designs (II)-(IX)) performed similarly across all histological grades, indicating that performance was somewhat invariant to histological grade.

Table 3: Runtime measurements of the proposed method, Mob-PW-UNet. Experiments were repeated ten times and respective average and standard deviation are reported in seconds. OpenVINO and TensorRT were used as inference engines for CPU and GPU inference, respectively.

	Patch-wise	Refinement	Total
OpenVINO	$57.32 \pm 0.20$	$0.75 \pm 0.01$	$58.07 \pm 0.20$
TensorRT	$39.88 \pm 0.62$	$0.38 \pm 0.00$	$40.26 \pm 0.62$

The best performing method, Mob-PW-UNet, took approximately  $\sim 58$  seconds to run on a representative  $\times 400$  WSI using the CPU (see Table 3). Using the GPU, runtime was reduced to 40.26 seconds. The patch-wise method dominated the overall runtime, with  $\sim 1\%$  of the total runtime being used on the refinement stage.

<sup>5</sup><https://github.com/Peter554/StainTools>

## 5. Discussion

In this paper, we have developed a pipeline for tumour segmentation of WSIs, called H2G-Net, using H&E-stained WSIs from a well-described cohort of breast cancer patients. We have presented each component in the pipeline and assessed the impact of each component in an ablation study. Using multiple guiding components, we significantly improved segmentation performance, while reducing disk storage requirements compared to traditional training pipelines.

The best performing architectures utilized both low and high-resolution information from the WSI. A similar approach is used by pathologists when separating the tumour from surrounding tissue. The low-resolution image provides a coarse outline of the tumour, whereas higher resolution is often necessary for accurate delineation.

### 5.1. Cascaded design and related work

For segmentation, using low-resolution as the first step could reduce total runtime by filtering patches during preprocessing. However, UNet-LR, a U-Net using only low-resolution information, results in low sensitivity and should therefore not be the first step for breast cancer segmentation. In this work, we used a patch-wise, high-resolution method as a first step to optimize detection. A U-Net could then be trained at a later stage to refine the produced heatmap, using both the heatmap and the low-resolution WSI as input. Using the heatmap generated from the patch-wise method alone, some areas of the tumour, such as areas with abundant stromal or fatty tissue, may not be recognized. We show that the network benefits from having the low-resolution image, together with the heatmap.

Tang *et al.* (2021) used a two-step procedure to perform instance segmentation of objects in the Cityscapes data set (Cordts *et al.*, 2016). These images have initial resolution of  $1024 \times 2048$  pixels, but the classes of interest can easily be distinguished at lower resolution. In contrast to our design, they first performed semantic segmentation on the low-resolution, before refining the initial segmentation using a patch-wise design. They also used overlapping predictions along the border of the initial segmentation. Their approach might be an interesting refinement method to further improve the segmentation performance of our resulting low-resolution segmentation.

A similar refinement approach to Tang *et al.* (2021) was used by Sornapudi *et al.* (2020) for cervical intraepithelial neoplasia segmentation of H&E stained WSIs. However, introducing a new network for border refinement will make the overall runtime longer and introduce more complexity to the final pipeline. Isensee *et al.* (2021) conducted a similar two-step procedure for medical volumetric data. They first used a CAE applied on the downsampled version of the full 3D volume (CT/MRI). They then applied a 3D patch-wise refinement model, using both the local volumetric data (CT/MRI) and predicted heatmap as input.

Another similar architecture design to ours, was proposed by Nazeri *et al.* (2018) for WSI classification of breast cancer. They also used a patch-wise model in the first step, before feeding the resulting heatmap to a second CNN that performed WSI-level classification. In addition, they used skip connections to propagate learned features from the patch-wise CNN to the latter CNN. Thus, our method could be seen as an adaption to their design applied to image segmentation. This style of skip connection is similar to the Double U-net approach by Jha *et al.* (2020). In this study, we did not explore skipping features from the classifier to the refinement network. This could be explored in future work. Our design is also similar to the work of Daly *et al.* (2020), where a similar two-stage, cascaded CNN design was deployed, but for image registration of WSIs.

### 5.2. Architecture depth, clustering, and patch generation

An interesting observation in this study is that using the deepest and most complex network for tumour segmentation is not necessarily better. From Table 1, we observe that InceptionV3 outperformed MobileNetV2 without any of the proposed guiding methods. However, we can achieve similar accuracy to InceptionV3, in addition to reduced inference memory usage and runtime, by using cluster-guiding with the MobileNetV2 architecture. A similar trend could be seen from the refinement network. Choosing more complex CAEs did not significantly improve segmentation performance. This could be due to data that did not cover all possible variations. The quality of the heatmap provided from the detection stage varied in some cases, making it challenging for the refinement network to improve the initial segmentation.

Reading patches from the raw WSI format is time consuming. It is therefore common to preprocess data before training. In this study, we sampled patches directly from the raw WSI format during training. This idea was recently proposed by Lutnick *et al.* (2021). We further extended on their idea to make it more generic. The approach by Lutnick *et al.* (2021) cannot handle larger batch sizes, as the cost of batch generation is not scalable. Thus, we used accumulated gradients to speed up batch generation, while simultaneously reducing GPU memory usage. We further introduced the concept of hierarchical sampling, which added direct support for balancing on multiple categories and labels. This design also added direct support for performing cluster-balancing end-to-end during training. Even though our design did not benefit from the clustering method used, the clustering method could easily be substituted.

### 5.3. Future perspectives

No benefit from using cluster-guiding to detect breast cancer tissue was observed, comparing Mob-KM-PW and Mob-PW by qualitative visual inspection. This was also observed in a study by Kaiser *et al.* (2019). They demonstrated improved performance by using a more advanced



clustering approach. Thus, in future work, substituting the ImageNet features + PCA +  $k$ -means clustering approach with a more suited clustering design should be explored. Given a suitable clustering approach, a natural next step could be to provide the predicted cluster heatmap with the confidence map, as it would provide different, representation-informative, high-resolution information to the refinement network.

Multiple instance learning (MIL) is a promising approach that tackles the challenge of weak supervision and noisy ground truth (Ilse *et al.*, 2018). Exchanging the MIL design with the single-instance CNN classifier is possible. In this framework, one could still perform clustering in pre-processing, and sample patches to the bag, as done in a recent study (Yao, Zhu, Jonnagaddala, *et al.*, 2020). However, an interesting approach proposed by Xu *et al.* (2012) was to perform clustering directly within the MIL design on bag-level. Using attention, one could train a network, not only to solve a task, but to learn subcategory structures in the data, while simultaneously filtering redundant clusters and noisy patches. This was demonstrated by M. Y. Lu *et al.* (2021). However, they did not assess the impact of the clustering component. Future work should involve replacing the single-instance CNN with the MIL design, incorporating clustering in an end-to-end fashion, and properly assessing its impact.

#### 5.4. Strengths and limitations

The main strengths of the study are that the models were trained on a large set of breast cancer WSIs. Tumour annotations were created in a (semi-)automatic manner, and manually corrected by pathologists. To ensure consistency, all annotations were assessed by a pathologist experienced in breast cancer pathology. Validation studies were conducted using an independent test set. The performance of the different designs was also evaluated for each histological grade separately. An ablation study was performed to assess the impact of each component in the multi-step pipeline. The proposed design was validated against baseline methods, and the best method was integrated in an open platform, FastPathology (Pedersen *et al.*, 2021).

The main limitations are that the models were trained using sections that were H&E-stained in the same laboratory and scanned in a single scanner. We demonstrated that the model generalized well to the test set, however, we have not tested our model on WSIs from other institutions. It is possible to carry out data augmentation to make the models more invariant, but it is challenging to mimic different staining and scanning effects (Tellez *et al.*, 2019). Thus, in the future, data from different laboratories and scanners will be added for training the models. We did not perform stain normalization as it would have added an additional layer of uncertainty and dependency in the pipeline. Furthermore, it would be interesting to assess the extent of generalization capability of our models

to cancers of other origins, such as lung or gastrointestinal cancer.

## 6. Conclusion

Through our hybrid guiding scheme, we demonstrated a significant improvement in segmentation of breast cancer tumours from gigapixel histopathology images. The model outperformed single resolution approaches, and introduced a simple, fast, and accurate way to refine segmentation heatmaps, without the need for overlapping inference or ensembling. We also presented a hierarchical sampling scheme, that enabled patches to be streamed from the raw WSI format concurrently during training. Furthermore, we demonstrated that tissue type balancing can be performed end-to-end, using a novel loss function. The hierarchical sampling scheme and the novel loss function were introduced to make training methods more scalable and to reduce storage requirements.

## Authors' contribution

André Pedersen: Conceptualization, Methodology, Investigation, Annotation, Writing – original draft, Writing - review & editing, Software, Validation. Erik Smistad: Methodology, Investigation, Supervision, Writing – original draft, Writing - review & editing, Software. Tor V. Rise: Annotation, Writing - review & editing, Pathology expertise. Vibeke G. Dale: Annotation, Writing - review & editing, Pathology expertise. Henrik S. Pettersen: Annotation, Writing - review & editing, Pathology expertise. David Bouget: Methodology, Supervision, Writing - original draft, Writing - review & editing. Tor-Arne S. Nordmo: Methodology, Investigation, Writing - review & editing. Ingerid Reinertsen: Conceptualization, Methodology, Supervision, Writing - original draft, Writing - review & editing. Marit Valla: Conceptualization, Methodology, Investigation, Annotation, Supervision, Data curation, Writing - original draft, Writing - review & editing, Resources, Pathology expertise, Project administration. All authors reviewed and approved the final version of the manuscript.

## Funding

This work was supported by The Liaison Committee for Education, Research and Innovation in Central Norway [grant number 2018/42794]; The Joint Research Committee between St. Olavs hospital and the Faculty of Medicine and Health Sciences, NTNU (FFU) [grant number 2019/38882]; The Cancer Foundation, St. Olavs hospital, Trondheim University Hospital [grant number 13/2021]; and The Clinic of Laboratory Medicine, St. Olavs hospital, Trondheim University Hospital [grant number 2020/14728-49].

## Conflicts of interest statement

The authors declare no conflict of interest.

## References

- Abadi, Martin, Paul Barham, Jianmin Chen, *et al.* (2016). “Tensorflow: A system for large-scale machine learning”. In: *12th {USENIX} Symposium on Operating Systems Design and Implementation ({OSDI} 16)*, pp. 265–283.
- Aresta, Guilherme, Teresa Araújo, Scotty Kwok, *et al.* (2019). “BACH: Grand challenge on breast cancer histology images”. In: *Medical Image Analysis* 56, pp. 122–139. ISSN: 1361-8415. DOI: <https://doi.org/10.1016/j.media.2019.05.010>. URL: <http://www.sciencedirect.com/science/article/pii/S1361841518307941>.
- Bai, Junjie, Fang Lu, Ke Zhang, *et al.* (2019). *ONNX: Open Neural Network Exchange*. <https://github.com/onnx/onnx>.
- Bándi, Péter, Maschenka Balkenhol, Bram Ginneken, *et al.* (Dec. 2019). “Resolution-agnostic tissue segmentation in whole-slide histopathology images with convolutional neural networks”. In: *PeerJ* 7, e8242. DOI: [10.7717/peerj.8242](https://doi.org/10.7717/peerj.8242).
- Bankhead, Peter, Maurice Loughrey, Jose Fernandez, *et al.* (Dec. 2017). “QuPath: Open source software for digital pathology image analysis”. In: *Scientific Reports* 7. DOI: [10.1038/s41598-017-17204-5](https://doi.org/10.1038/s41598-017-17204-5).
- Bouget, David, André Pedersen, Sayied Abdol Mohieb Hossainy, *et al.* (2021). “Meningioma segmentation in t1-weighted mri leveraging global context and attention mechanisms”. In: *arXiv preprint arXiv:2101.07715*.
- Carse, Jacob and Stephen McKenna (July 2019). “Active Learning for Patch-Based Digital Pathology Using Convolutional Neural Networks to Reduce Annotation Costs”. In: pp. 20–27. DOI: [10.1007/978-3-030-23937-4\\_3](https://doi.org/10.1007/978-3-030-23937-4_3).
- Cordts, Marius, Mohamed Omran, Sebastian Ramos, *et al.* (2016). “The Cityscapes Dataset for Semantic Urban Scene Understanding”. In: *Proc. of the IEEE Conference on Computer Vision and Pattern Recognition (CVPR)*.
- Daly, Aidan, Krzysztof Geras, and Richard Bonneau (Sept. 2020). “A convolutional neural network for common coordinate registration of high-resolution histology images”. In: DOI: [10.1101/2020.09.18.303875](https://doi.org/10.1101/2020.09.18.303875).
- Deng, Jia, Wei Dong, Richard Socher, *et al.* (2009). “Imagenet: A large-scale hierarchical image database”. In: *2009 IEEE conference on computer vision and pattern recognition*. Ieee, pp. 248–255.
- Ehteshami Bejnordi, Babak, Mitko Veta, Johannes P, *et al.* (Dec. 2017). “Diagnostic Assessment of Deep Learning Algorithms for Detection of Lymph Node Metastases in Women With Breast Cancer”. In: *JAMA* 318, pp. 2199–2210. DOI: [10.1001/jama.2017.14585](https://doi.org/10.1001/jama.2017.14585).
- Elston, C. and I. Ellis (1991). “pathological prognostic factors in breast cancer. I. The value of histological grade in breast cancer: experience from a large study with long-term follow-up”. In: *Histopathology* 19.
- Engstrøm, Monica, Signe Opdahl, Anne Hagen, *et al.* (July 2013). “Molecular subtypes, histopathological grade and survival in a historic cohort of breast cancer patients”. In: *Breast cancer research and treatment* 140. DOI: [10.1007/s10549-013-2647-2](https://doi.org/10.1007/s10549-013-2647-2).
- Ferlay, J, M Ervik, F Lam, *et al.* (2020). *Global Cancer Observatory: Cancer Today*. Lyon: International Agency for Research on Cancer. Last accessed 2021-04-21. URL: <https://gco.iarc.fr/today>.
- Guo, Zichao, Hong Liu, Haomiao Ni, *et al.* (Dec. 2019). “A Fast and Refined Cancer Regions Segmentation Framework in Whole-slide Breast Pathological Images”. In: *Scientific Reports* 9, p. 882. DOI: [10.1038/s41598-018-37492-9](https://doi.org/10.1038/s41598-018-37492-9).
- Ilse, Maximilian, Jakub Tomczak, and Max Welling (July 2018). “Attention-based Deep Multiple Instance Learning”. In: *Proceedings of the 35th International Conference on Machine Learning*. Ed. by Jennifer Dy and Andreas Krause. Vol. 80. Proceedings of Machine Learning Research. PMLR, pp. 2127–2136. URL: <http://proceedings.mlr.press/v80/ilse18a.html>.
- Intel (2019). *OpenVINO Toolkit*. Last accessed 2019-06-10. URL: <https://software.intel.com/openvino-toolkit>.
- Ioffe, Sergey and Christian Szegedy (2015). “Batch Normalization: Accelerating Deep Network Training by Reducing Internal Covariate Shift”. In: *Proceedings of the 32nd International Conference on International Conference on Machine Learning - Volume 37*. ICML’15. Lille, France: JMLR.org, pp. 448–456.
- Isensee, Fabian, Paul Jaeger, Simon Kohl, *et al.* (Feb. 2021). “nnU-Net: a self-configuring method for deep learning-based biomedical image segmentation”. In: *Nature Methods* 18, pp. 1–9. DOI: [10.1038/s41592-020-01008-z](https://doi.org/10.1038/s41592-020-01008-z).
- Jha, Debesh, Michael Riegler, Dag Johansen, *et al.* (July 2020). “DoubleU-Net: A Deep Convolutional Neural Network for Medical Image Segmentation”. In: pp. 558–564. DOI: [10.1109/CBMS49503.2020.00111](https://doi.org/10.1109/CBMS49503.2020.00111).
- Kamnitsas, Konstantinos, Christian Ledig, Virginia F.J. Newcombe, *et al.* (2017). “Efficient multi-scale 3D CNN with fully connected CRF for accurate brain lesion segmentation”. In: *Medical Image Analysis* 36, pp. 61–78. ISSN: 1361-8415. DOI: <https://doi.org/10.1016/j.media.2016.10.004>. URL: <https://www.sciencedirect.com/science/article/pii/S1361841516301839>.
- Karl Pearson, F.R.S. (1901). “LIII. On lines and planes of closest fit to systems of points in space”. In: *The London, Edinburgh, and Dublin Philosophical Magazine and Journal of Science* 2.11, pp. 559–572. DOI: [10.1080/14786440109462720](https://doi.org/10.1080/14786440109462720). eprint: <https://doi.org/10.1080/14786440109462720>.

- 1080/14786440109462720. URL: <https://doi.org/10.1080/14786440109462720>.
- Kassani, Sara Hosseinzadeh, Peyman Hosseinzadeh Kassani, Michal J. Wesolowski, *et al.* (2019). “Classification of Histopathological Biopsy Images Using Ensemble of Deep Learning Networks”. In: *Proceedings of the 29th Annual International Conference on Computer Science and Software Engineering*. CASCON '19. IBM Corp., pp. 92–99.
- Kingma, Diederik and Jimmy Ba (Dec. 2014). “Adam: A Method for Stochastic Optimization”. In: *International Conference on Learning Representations*. URL: <https://arxiv.org/abs/1412.6980>.
- Lu, Ming Y., Drew F. K. Williamson, Tiffany Y. Chen, *et al.* (2021). “Data-efficient and weakly supervised computational pathology on whole-slide images”. In: *Nature Biomedical Engineering*. DOI: [10.1038/s41551-020-00682-w](https://doi.org/10.1038/s41551-020-00682-w). URL: <https://doi.org/10.1038/s41551-020-00682-w>.
- Lutnick, Brendon, Leema Krishna Murali, Brandon Gingley, *et al.* (2021). *Histo-fetch – On-the-fly processing of gigapixel whole slide images simplifies and speeds neural network training*. arXiv: [2102.11433](https://arxiv.org/abs/2102.11433) [eess.IV].
- Macenko, Marc, Marc Niethammer, J. S. Marron, *et al.* (2009). “A method for normalizing histology slides for quantitative analysis”. In: *2009 IEEE International Symposium on Biomedical Imaging: From Nano to Macro*, pp. 1107–1110. DOI: [10.1109/ISBI.2009.5193250](https://doi.org/10.1109/ISBI.2009.5193250).
- Minaee, Shervin, Yuri Y. Boykov, Fatih Porikli, *et al.* (2021). “Image Segmentation Using Deep Learning: A Survey”. In: *IEEE Transactions on Pattern Analysis and Machine Intelligence*, pp. 1–1. DOI: [10.1109/TPAMI.2021.3059968](https://doi.org/10.1109/TPAMI.2021.3059968).
- Nazeri, Kamyar, Azad Aminpour, and Mehran Ebrahimi (June 2018). “Two-Stage Convolutional Neural Network for Breast Cancer Histology Image Classification”. In: pp. 717–726. ISBN: 978-3-319-92999-6. DOI: [10.1007/978-3-319-93000-8\\_81](https://doi.org/10.1007/978-3-319-93000-8_81).
- Nie, Dong, Li Wang, Roger Trullo, *et al.* (Sept. 2017). “Segmentation of Craniomaxillofacial Bony Structures from MRI with a 3D Deep-Learning Based Cascade Framework”. In: vol. 10541, pp. 266–273. ISBN: 978-3-319-67388-2. DOI: [10.1007/978-3-319-67389-9\\_31](https://doi.org/10.1007/978-3-319-67389-9_31).
- NVIDIA (2019). *TensorRT*. Last accessed 2019-06-10. URL: <https://developer.nvidia.com/tensorrt>.
- Otsu, N. (Jan. 1979). “A Threshold Selection Method from Gray-Level Histograms”. In: *IEEE Transactions on Systems, Man, and Cybernetics* 9.1, pp. 62–66. ISSN: 2168-2909. DOI: [10.1109/TSMC.1979.4310076](https://doi.org/10.1109/TSMC.1979.4310076).
- Painchaud, Nathan, Youssef Skandarani, Thierry Judge, *et al.* (2019). “Cardiac MRI Segmentation with Strong Anatomical Guarantees”. In: *Medical Image Computing and Computer Assisted Intervention – MICCAI 2019*. Ed. by Dinggang Shen, Tianming Liu, Terry M. Peters, *et al.* Cham: Springer International Publishing, pp. 632–640. ISBN: 978-3-030-32245-8.
- Pedersen, André, Marit Valla, Anna M. Bofin, *et al.* (Apr. 2021). “FastPathology: An Open-Source Platform for Deep Learning-Based Research and Decision Support in Digital Pathology”. In: *IEEE Access* 9, pp. 58216–58229. DOI: [10.1109/ACCESS.2021.3072231](https://doi.org/10.1109/ACCESS.2021.3072231).
- Pedregosa, F., G. Varoquaux, A. Gramfort, *et al.* (2011). “Scikit-learn: Machine Learning in Python”. In: *Journal of Machine Learning Research* 12, pp. 2825–2830.
- Priego Torres, Blanca, Daniel Morillo, Miguel Angel Granero, *et al.* (Mar. 2020). “Automatic Segmentation of Whole-Slide H&E Stained Breast Histopathology Images using a Deep Convolutional Neural Network Architecture”. In: *Expert Systems with Applications* 151, p. 113387. DOI: [10.1016/j.eswa.2020.113387](https://doi.org/10.1016/j.eswa.2020.113387).
- Qaiser, Talha, Yee-Wah Tsang, Daiki Taniyama, *et al.* (2019). “Fast and accurate tumor segmentation of histology images using persistent homology and deep convolutional features”. In: *Medical Image Analysis* 55, pp. 1–14. ISSN: 1361-8415. DOI: <https://doi.org/10.1016/j.media.2019.03.014>. URL: <https://www.sciencedirect.com/science/article/pii/S1361841518302688>.
- Redmon, Joseph and Ali Farhadi (2018). “YOLOv3: An Incremental Improvement”. In: *CoRR* abs/1804.02767. arXiv: [1804.02767](https://arxiv.org/abs/1804.02767). URL: <http://arxiv.org/abs/1804.02767>.
- Ronneberger, Olaf, Philipp Fischer, and Thomas Brox (2015). “U-Net: Convolutional Networks for Biomedical Image Segmentation”. In: *Medical Image Computing and Computer-Assisted Intervention – MICCAI 2015*. Ed. by Nassir Navab, Joachim Hornegger, William M. Wells, *et al.* Cham: Springer International Publishing, pp. 234–241.
- Russakovsky, Olga, Jia Deng, Hao Su, *et al.* (2015). “ImageNet Large Scale Visual Recognition Challenge”. In: *International Journal of Computer Vision (IJCV)* 115.3, pp. 211–252. DOI: [10.1007/s11263-015-0816-y](https://doi.org/10.1007/s11263-015-0816-y).
- Sandler, Mark, Andrew Howard, Menglong Zhu, *et al.* (2018). “MobileNetV2: Inverted Residuals and Linear Bottlenecks”. In: *2018 IEEE/CVF Conference on Computer Vision and Pattern Recognition*, pp. 4510–4520. DOI: [10.1109/CVPR.2018.00474](https://doi.org/10.1109/CVPR.2018.00474).
- Satyanarayanan, Mahadev, Adam Goode, Benjamin Gilbert, *et al.* (2013). “OpenSlide: A vendor-neutral software foundation for digital pathology”. In: *Journal of Pathology Informatics* 4.1, p. 27. ISSN: 2153-3539. DOI: [10.4103/2153-3539.119005](https://doi.org/10.4103/2153-3539.119005). URL: <http://www.jpathinformatics.org/text.asp?2013/4/1/27/119005>.
- Schmitz, Rüdiger, Frederic Madesta, Maximilian Nielsen, *et al.* (2021). “Multi-scale fully convolutional neural networks for histopathology image segmentation: From nuclear aberrations to the global tissue architecture”. In: *Medical Image Analysis* 70, p. 101996. ISSN: 1361-8415. DOI: <https://doi.org/10.1016/j.media.2021.101996>.

101996. URL: <https://www.sciencedirect.com/science/article/pii/S1361841521000426>.
- Simonyan, Karen and Andrew Zisserman (2015). “Very Deep Convolutional Networks for Large-Scale Image Recognition”. In: *International Conference on Learning Representations*. URL: <https://www.robots.ox.ac.uk/~vgg/publications/2015/Simonyan15/simonyan15.pdf>.
- Skrede, Ole-Johan, Sepp De Raedt, Andreas Kleppe, *et al.* (Feb. 2020). “Deep learning for prediction of colorectal cancer outcome: a discovery and validation study”. In: *The Lancet* 395, pp. 350–360. DOI: [10.1016/S0140-6736\(19\)32998-8](https://doi.org/10.1016/S0140-6736(19)32998-8).
- Smistad, Erik, Andreas Østvik, and André Pedersen (Sept. 2019). “High performance neural network inference, streaming and visualization of medical images using FAST”. In: *IEEE Access* PP, pp. 1–1. DOI: [10.1109/ACCESS.2019.2942441](https://doi.org/10.1109/ACCESS.2019.2942441).
- Sornapudi, Sudhir, Ravitej Addanki, Ronald Stanley, *et al.* (July 2020). “Cervical Whole Slide Histology Image Analysis Toolbox”. In: DOI: [10.1101/2020.07.22.20160366](https://doi.org/10.1101/2020.07.22.20160366).
- Srinidhi, Chetan L., Ozan Ciga, and Anne L. Martel (2021). “Deep neural network models for computational histopathology: A survey”. In: *Medical Image Analysis* 67, p. 101813. ISSN: 1361-8415. DOI: <https://doi.org/10.1016/j.media.2020.101813>. URL: <https://www.sciencedirect.com/science/article/pii/S1361841520301778>.
- Srivastava, Nitish, Geoffrey E. Hinton, A. Krizhevsky, *et al.* (2014). “Dropout: a simple way to prevent neural networks from overfitting”. In: *J. Mach. Learn. Res.* 15, pp. 1929–1958.
- Steinhaus, Hugo (1956). “Sur la division des corps matériels en parties”. In: *Bulletin de l’Académie Polonaise des Sciences* 12.4, pp. 801–804.
- Szegedy, Christian, Vincent Vanhoucke, Sergey Ioffe, *et al.* (June 2016). “Rethinking the Inception Architecture for Computer Vision”. In: DOI: [10.1109/CVPR.2016.308](https://doi.org/10.1109/CVPR.2016.308).
- Tang, Chufeng, Hang Chen, Xiao Li, *et al.* (Apr. 2021). “Look Closer to Segment Better: Boundary Patch Refinement for Instance Segmentation”. In: *ArXiv* abs/2104.05239.
- Tellez, David, Geert Litjens, Péter Bándi, *et al.* (2019). “Quantifying the effects of data augmentation and stain color normalization in convolutional neural networks for computational pathology”. In: *Medical Image Analysis* 58, p. 101544. ISSN: 1361-8415. DOI: <https://doi.org/10.1016/j.media.2019.101544>. URL: <https://www.sciencedirect.com/science/article/pii/S1361841519300799>.
- The Royal College of Pathologists (2018). *Meeting pathology demand: Histopathology workforce census*. Last accessed 2021-04-21. URL: <https://www.rcpath.org/uploads/assets/952a934d-2ec3-48c9-a8e6e00fcdca700f/Meeting-Pathology-Demand-Histopathology-Workforce-Census-2018.pdf>.
- Xu, Yan, Jun-Yan Zhu, Eric Chang, *et al.* (June 2012). “Multiple clustered instance learning for histopathology cancer image classification, segmentation and clustering”. In: *2012 IEEE Conference on Computer Vision and Pattern Recognition*, pp. 964–971. DOI: [10.1109/CVPR.2012.6247772](https://doi.org/10.1109/CVPR.2012.6247772).
- Yao, Jiawen, Xinliang Zhu, and Junzhou Huang (2019). “Deep Multi-instance Learning for Survival Prediction from Whole Slide Images”. In: *International Conference on Medical Image Computing and Computer-Assisted Intervention*. Springer, pp. 496–504.
- Yao, Jiawen, Xinliang Zhu, Jitendra Jonnagaddala, *et al.* (2020). “Whole slide images based cancer survival prediction using attention guided deep multiple instance learning networks”. In: *Medical Image Analysis* 65, p. 101789. ISSN: 1361-8415. DOI: <https://doi.org/10.1016/j.media.2020.101789>. URL: <https://www.sciencedirect.com/science/article/pii/S1361841520301535>.